Accretion Flow in Magnetic Cataclysmic Variables

Kinwah Wu[1] ⋆, Mark Cropper[1], Gavin Ramsay[1], Curtis Saxton[2] and Chris Bridge[1]

[1] Mullard Space Science Laboratory, University College London, Holmbury St Mary, Surrey, RH5 6NT, United Kingdom

[2] Max-Planck-Institute für Radioastronomie, Auf dem Hügel 69, D-53121 Bonn, Germany

Abstract The standard model of the post-shock accretion flow in mCVs is discussed. We present some results of the current study of two-temperature flows in mCVs. New observations supporting the standard model are presented. Recent developments in the studies of the global properties of the accretion stream are briefly discussed.

Key words: accretion, accretion disks – stars: binaries – stars: cataclysmic variables – X-rays: binaries

1 INTRODUCTION

Magnetic cataclysmic variables (mCVs) are close binaries in which a Roche-lobe filling low-mass companion star transfers material to a magnetic white dwarf. There are two main classes of mCVs: the AM Her systems (also known as polars) and the intermediate polars (see Fig. 1). In AM Her systems, the magnetic field of the white dwarf is strong enough to lock the whole system into synchronous (or almost synchronous) rotation. It also prevents the formation of an accretion disk and channels the accreting material directly to the white-dwarf magnetic pole(s). In intermediate polars (IPs), the white-dwarf magnetic field is weaker. There is an accretion disk around the white dwarf, but the inner disk is disrupted by the white-dwarf magnetic field, and the accretion flow is channeled by the field to the white-dwarf magnetic pole region(s). (See e.g. Warner 1995, Cropper 1990 for a review of mCVs.)

Here, we review the standard model of field-channeled accretion in mCVs. We organize the paper as follows. In §2 we discuss the hydrodynamics of the post-shock accretion flow, and in §3 we discuss the X-ray emission from the post-shock region and the observational consequences. In §4 we briefly discuss the current development in the study of the global properties of the accretion column/stream.

2 STANDARD MODEL FOR POST-SHOCK FLOW IN MCVS

In the standard model, the accretion flow in the upper accretion stream of a mCV is supersonic, and it becomes subsonic, via a strong shock, before reaching the white-dwarf surface. The shock
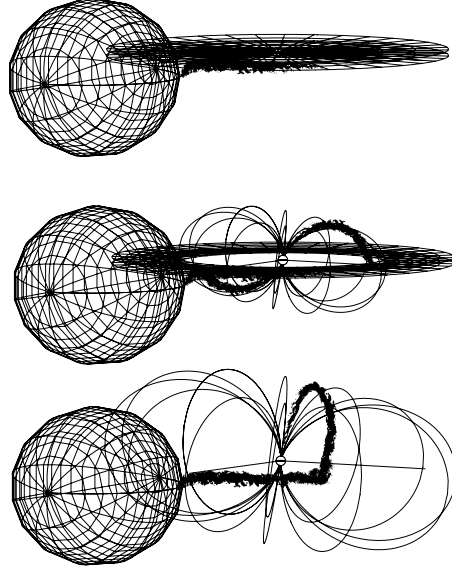
Fig. 1   Schematic illustration of different types of cataclysmic variable: a non-magnetic cataclysmic variable (top), an intermediate polar (middle) and an AM Her system (bottom). (Adapted from Cropper et al. 2002).

temperature, which depends mainly on the white-dwarf mass and radius, is given by

$$kT_{\mathrm{s}} \approx \frac{3}{8}\frac{\mu G M_{\mathrm{w}} m_{\mathrm{H}}}{R_{\mathrm{w}}} = 26 \left(\frac{\mu}{0.5}\right)\left(\frac{M_{\mathrm{w}}}{M_{\odot}}\right)\left(\frac{R_{\mathrm{w}}}{10^9\,\mathrm{cm}}\right)^{-1} \mathrm{keV} \ , \tag{1}$$

where G is the gravitational constant, m_{H} is the hydrogen mass, μ is the mean molecular weight, M_{w} is the white-dwarf mass, and R_{w} is the white-dwarf radius. The accretion shock heats and ionizes the accreting gas. The shock-heated gas is cooled down by emitting bremsstrahlung X-rays and optical/IR cyclotron radiation, when settling onto the white-dwarf atmosphere (Lamb & Masters 1979). The thickness of the post-shock emission region (the shock height) is approximately given by

$$x_{\mathrm{s}} \sim \frac{1}{4}v_{\mathrm{ff}}t_{\mathrm{cool}} \approx 6.4 \times 10^7 \left(\frac{M_{\mathrm{w}}}{0.5\,\mathrm{M_{\odot}}}\right)^{1/2}\left(\frac{R_{\mathrm{w}}}{10^9\,\mathrm{cm}}\right)^{-1/2}\left(\frac{t_{\mathrm{cool}}}{1\,\mathrm{s}}\right)\mathrm{cm} \ , \tag{2}$$

where t_{cool} is the cooling time and v_{ff} the free-fall velocity.

   The post-shock accretion flow is described by the hydrodynamic equations:

$$\frac{d}{dt}\rho + \rho\left(\nabla \cdot \boldsymbol{v}\right) = 0 \ , \tag{3}$$

$$\frac{d}{dt}\boldsymbol{v} + \frac{1}{\rho}\nabla(P_{\mathrm{e}} + P_{\mathrm{i}}) = \boldsymbol{g} \ , \tag{4}$$

$$\frac{d}{dt}P_{\mathrm{i}} - \gamma\frac{P_{\mathrm{i}}}{\rho}\frac{d}{dt}\rho = -(\gamma - 1)\Gamma_{\mathrm{ei}} \ , \tag{5}$$
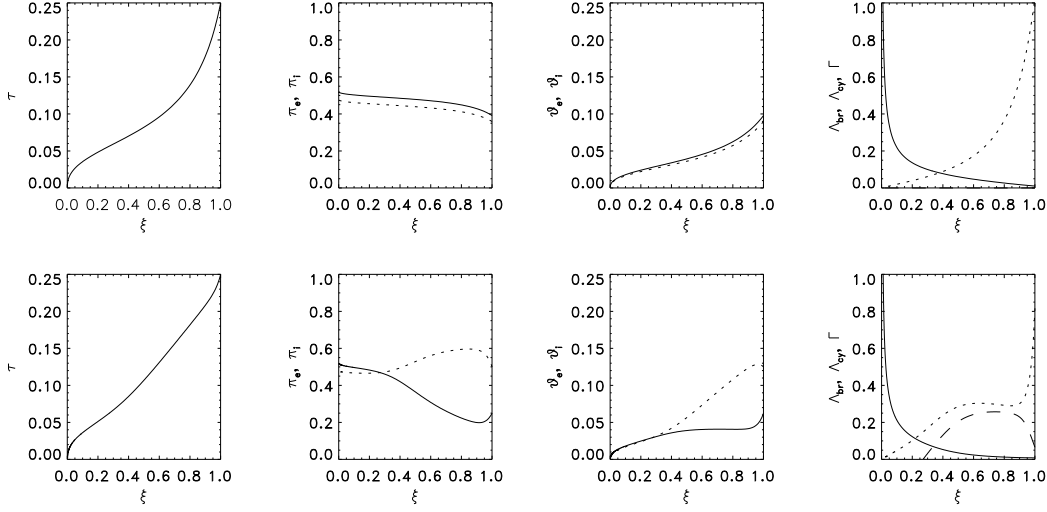
Fig. 2 Model one-temperature (top) and two-temperature (bottom) flows in the post-shock region dominated by cyclotron cooling. The ratio of the cyclotron cooling timescale to the bremsstrahlung cooling timescale $\epsilon_s = 100$ (see Wu 1994). In the two-temperature flow, the parameters are electron-ion coupling parameter at the shock $\sigma_s = 0.5$ and the parameter determining the electron-ion collisional timescale in the flow $\psi_{ei} = 0.5$ (see Saxton & Wu 2001 for details of these parameters). Solar abundances are assumed in both cases. The panels from left to right show the stationary profiles of the normalized flow velocity (τ), partial pressures of the electrons and the ions (π_e and π_i, solid and dotted lines respectively), electrons and ion temperatures (θ_e and θ_i solid and dotted lines respectively), and the bremsstrahlung cooling rate (Λ_{br}, solid line), cyclotron cooling rate (Λ_{cy}, dotted line) and the electron-ion exchange rate Γ (dashed line). The velocity is normalized to v_{ff}, the free-fall velocity at the white-dwarf surface. The electron and ion partial pressures are normalized to $\rho_a v_{ff}^2$ where ρ_a is the density of pre-shock flow. The electrons and ion temperatures are normalized to $m_e c^2/k_B$ and $m_i c^2/k_B$ respectively, where m_e and m_i are electron and ion masses, c is the speed of light and k_B is the Boltzmann constant. The normalizations of the cooling rates are more complicated and can be found in Satxon & Wu (1999, 2001). The white dwarf surface is at $\xi = 0$, and the shock is at $\xi = 1$.

$$\frac{d}{dt}P_e - \gamma\frac{P_e}{\rho}\frac{d}{dt}\rho = -(\gamma-1)\big[\nabla\cdot\boldsymbol{F}_{rad} - \Lambda_h - \Gamma_{ei}\big] \tag{6}$$

($d/dt \equiv \partial/\partial t + \boldsymbol{v}\cdot\nabla$), where P_e, P_i, $\boldsymbol{v}$ and ρ are the electron pressure, ion pressure, velocity and density. γ is the adiabatic index of the gas, $\boldsymbol{g}$ is the gravitational force, $\boldsymbol{F}_{rad}$ is the radiative flux, Γ_{ei} is the electron-ion energy exchange term, and Λ_h is the heating function. These equations are coupled to the radiative-transfer equation

$$(\boldsymbol{n}\cdot\nabla)I(\boldsymbol{r},\boldsymbol{n},\nu) = -\chi(\boldsymbol{r},\boldsymbol{n},\nu)I(\boldsymbol{r},\boldsymbol{n},\nu) + \eta(\boldsymbol{r},\boldsymbol{n},\nu) , \tag{7}$$

where I is the intensity of the radiation, χ is the extinction coefficient, η is the emissivity, and $\boldsymbol{n}$ is the normal vector of the radiation propagation. (For a more detail discussion of the hydrodynamics of accretion flow in mCVs, see Wu 2000 and references therein; see also Imamura et al. 1987, 1996 and Woelk & Beuermann 1996.)

Near the white-dwarf surface the accretion is channelled by the magnetic field, and the flow is practically one-dimensional. For post-shock accretion in mCVs, we may consider an approximation in which the radiative energy transport term $\nabla \cdot \boldsymbol{F}_{\mathrm{rad}}$ can be combined with the heating term Λ_{h} and be replaced by an effective cooling term Λ_{eff} (see Saxton 1999). Under this approximation the hydrodynamic equations are decoupled from the radiative-transfer equations. For systems with very strong radiative cooling, the shock height x_{s} will be much smaller than the white-dwarf radius R_{w}. In this case, we may use the "thin-shock" approximation and omit gravity effects in the hydrodynamic calculations. We note that the thin-shock approximation is not valid, for systems with a very massive white dwarf and a low magnetic field (Cropper et al. 1999).

Generally, the Rankine-Hugoniot jump conditions are assumed at the shock and a cold stationary wall boundary condition ($v = 0$ and $T = 0$) at the white-dwarf surface (e.g. Chevalier & Imamura 1982 and Wu, Chanmugam & Shaviv 1994; see also Imamura et al. 1996; Wu & Cropper 2001; Saxton 2002 for alternative lower boundary conditions). With the boundary conditions specified, the hydrodynamic equations can be solved to obtain the structures of the post-shock region.

For a stationary flow, we ignore the partial time derivatives in the hydrodynamic equations. If the electron-ion exchange time scale is much shorter than the dynamical and radiative cooling timescales, we eliminate the electron-ion exchange term Γ_{ei} by combining the electron-energy and ion-energy equations into a single equation:

$$(\boldsymbol{v} \cdot \nabla)P - \gamma \frac{P}{\rho}(\boldsymbol{v} \cdot \nabla)\rho = -(\gamma - 1)\Lambda_{\mathrm{eff}} \ . \tag{8}$$

This is known as the one-temperature approximation. When the electron-ion exchange time scale is comparable or longer than the cooling timescale, a full two-temperature treatment is required, and both the electron-energy and the ion-energy equations must be solved together. Generally, two-temperature flows occur in systems with a massive white dwarf and a strong magnetic field. Moreover, the specific accretion rate needs to be sufficiently low so that two-body collisional processes are inefficient. For high shock temperatures and strong magnetic fields, cyclotron loss is efficient, and the electrons in the post-shock region can be cooled very rapidly. Yet because of low gas density, electron-ion collision cannot maintain an efficient thermal coupling so that the radiatively cooled electrons can acquire energy from the shock-heated ions efficiently.

In Fig.2, we show the structures of two model post-shock regions obtained from the hydrodynamic calculations described above. In both cases the radiative loss is dominated by cyclotron cooling. We use an effective cooling function as that given in Wu (1994) and Wu, Chanmugam & Shaviv (1994) with solar abundances for the gas. The first one has a high electron-ion collision rate, and the electrons and ions maintain a similar temperature profile. The flow is thus one-temperature. The second one has an inefficient electron-ion energy exchange. The electrons and ions are weakly thermal coupled, and the flow is two-temperature. Despite the fact that the other system parameters are the same, the velocity, density and temperature structures of the two model flows are very different. The differences are most prominent in the regions near the shock. One can see clearly in the two-temperature flow that the ion temperatures are significantly higher than the electron temperatures in large fraction of the whole post-shock region. In those regions, the gas density is relatively low, where two-body processes such as electron-ion collision are inefficient. However, the properties of the one-temperature and two-temperature flows are similar in the bottom of the post-shock region, when the density becomes high enough for efficient electron-ion energy exchange to occur.
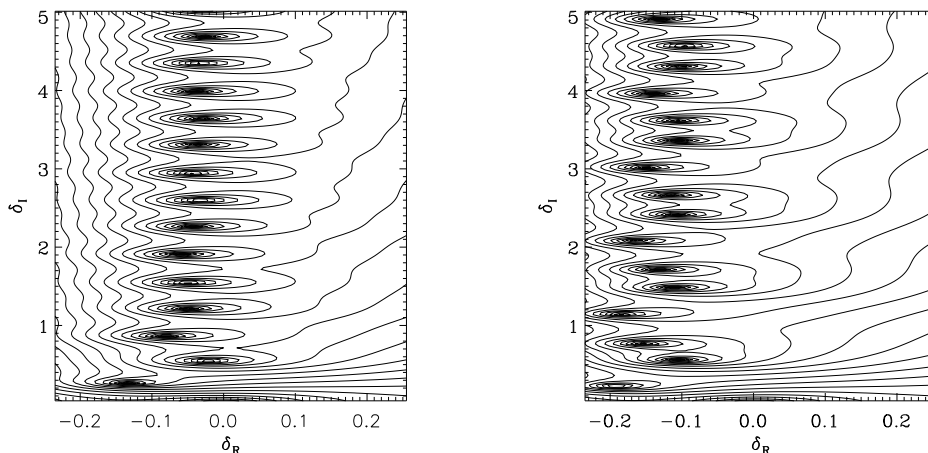
Fig. 3 The eigen plane of time-dependent linear analysis the flows in Fig. 2. The real part of the eigen value δ_R determine the stability, and the imaginary part of the eigen value δ_I determine the oscillation frequencies.

One-temperature flows and two-temperature flows also show different stability properties. Linear analyses (e.g. Chevalier & Imamura 1982; Saxton et al. 1998) and numerical simulations (e.g. Langer, Chanmugam & Shaviv 1982; Imamura, Wolff & Durisen 1984; Wu, Chanmugam & Shaviv 1992) show that one-temperature flows with bremsstrahlung cooling are thermal unstable. The flows are, however, thermally stable in the presence of cooling processes with stronger temperature dependence. Cyclotron cooling depends strongly on the electron temperature (see e.g. Wada et al. 1980; Chanmugam et al. 1989); thus, one-temperature flows are thermally stable when cyclotron radiation is the dominant cooling process. The thermal stability properties of two-temperature flows are more complicated, as the energy transport process involves both radiative loss and electron-ion exchange (Imamura et al. 1996; Saxton & Wu 2001). The energy exchange between electrons and ions can induce oscillations in the flow and causes instability even in the presence of strong cyclotron cooling. In some situations, the post-shock region is effectively separated into two zones, one of which electrons and ions are thermally coupled and another the two type of charge particles are weakly coupled, and the lower boundary condition loses its effect. As a consequence, the eigen frequencies of the oscillations are modified and the stability of the flow is altered (see Saxton & Wu 1999, 2001; Saxton 1999, 2002 for details). As an illustration we show in Fig.3 the eigen planes obtained from the time-dependent linear analyses of the two model flows that we have presented in Fig.2. One can easily see the shifts in both the real (stability) and imaginary (oscillatory) parts of the eigen frequencies of the oscillations when the electron-ion collision becomes inefficient.

3 X-RAY EMISSION PROPERTIES

The standard model has provided satisfactory explanations to many observations, in particular, the time-dependent optical/IR polarization light curves and spectra of AM Her systems (e.g. Wu & Wickramasinghe 1990) and the keV X-ray continuum of AM Her systems and IPs (Ishida

1991; Cropper, Ramsay & Wu 1998). In spite of its success, it has been argued that realistic post-shock accretion flows in mCVs may not resemble the hydrodynamic scenario described by the standard model. The arguments came from both theoretical and observational perspectives. The specific accretion rate across the accretion column could vary significantly. The thickness of the post-shock region depends on the cooling length, which decreases with increasing gas density. When the accretion rate varies across the accretion column, the shock height also varies across the column accordingly. Such variations in the shock height cause a large curvature in the shock surface. In the presence of a magnetic field, it is difficult for such severely curved shock surface to be stationary and stable. It has been argued that the accretion flow near the white dwarf is clumpy, consisting of dense blobs which are formed as a result of instability in the flow upstream (Kuijper & Pringle 1982; see Frank, King & Raine 2002). These dense blobs can penetrate deeply into the white-dwarf atmosphere and release the gravitational energy at large optical depths. The accretion poles of the the white dwarf bombarded by these dense blobs would emit optically thick soft X-rays, with a blackbody spectrum typical of a temperature $\sim 100\,\mathrm{eV}$. The clumpy scenario is in contrast to the standard model, in which a shock is formed above the white-dwarf atmosphere, heating the gas to emit optically thin bremsstrahlung continuum and bound-bound transition line emission in the keV energies and the post-shock flow is relatively smooth.

In the observational aspect, *EXOSAT* observations of AM Her systems showed large amplitude flickerings in the X-ray light curves (Heise et al. 1985). Such flickerings are difficult to be explained by models assuming a smooth accretion flow and a stationary shock. Moreover, the system AM Her itself (Heise et al. 1985) showed two very distinguishable accretion poles, one of which emitted only blackbody soft X-rays and another emitted keV hard X-rays. The presence of a strong soft X-ray pole is not predicted by the standard model either. Later *ROSAT* observations also indicated that the majority of AM Her systems have a soft blackbody component which dominates the total X-ray emission (Ramsay et al. 1994). The large soft/hard X-ray ratio posed more difficulties to the standard model, as it interprets the soft X-rays as radiation reprocessed from the hard X-rays emitted from the shock-heated accreting gas.

The large-amplitude X-ray variations, the presence of a soft X-ray pole and the large soft/hard X-ray ratio are, however, easily explained with the clumpy accretion model. The validity of the standard model has been under debate. Some issues regarding the standard model is eventually clarified by the new data obtained by *XMM-Newton* observations and by reanalysis of the *ROSAT* data.

The temperatures of the accretion shocks in mCVs are about $10 - 40\,\mathrm{keV}$. These temperatures are high enough to almost fully ionize the accreting gas. As the shock-heated gas is cooled along the flow, the post-shock region becomes stratified in temperature and density (see Fig.2). While the more highly ionized species are in the hot strata near the shock, the less ionized species are in cooler strata at the bottom. Moreover, because of density stratification, the relative abundances of the ions vary with heights in the emission region. The X-ray lines from the different ion species are therefore useful diagnostics to the structures of post-shock flows (Fujimoto & Ishida 1997; Wu, Cropper & Ramsay 2001). One may also use it to determine the masses of the accreting white dwarfs as the shock temperature one of the key parameters to determine the structure of the shock-heated emission region (Fujimoto & Ishida 1997; Tennant et al 1998; Cropper et al. 2001).

Figure 4 shows the *XMM-Newton* RGS spectrum of the IP EX Hya in the $0.5 - 2$ keV band (Cropper et al. 2002). When a parametric single-component optically thin thermal plasmas MEKAL model (Mewe, Kaastra & Liedahl 1995; Phillips et al. 1999) is used to fit the data, the residuals in the emission lines are obvious. Using a parametric three-component MEKAL
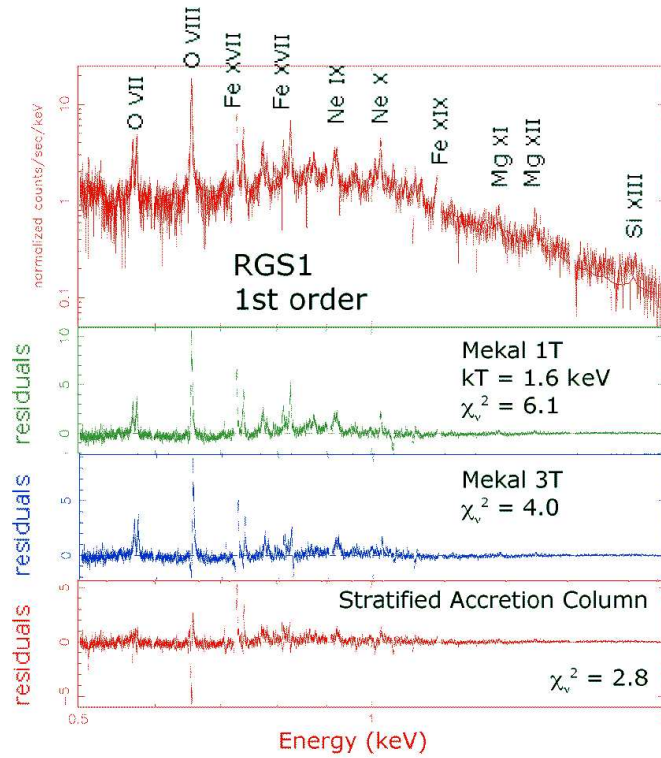
Fig. 4 The *XMM-Newton* RGS spectrum of the IP EX Hya showing the most prominent emission lines (adopted from Cropper et al. 2002). (a) Data and best-fit model spectrum obtained from the hydrodynamic model (see Cropper et al. 1999 for details). (b) The residuals of the fit when we use a homogeneous parametric model with one constant temperature component. (c) The residuals of the fit when we use a homogeneous parametric model with three constant temperature components. (d) The residuals of the fit when we use the hydrodynamic model.

model improves the fit, but the emission lines are still not explained to satisfaction. However, when a model spectrum for an optically thin plasma with density and temperature structures obtained from the hydrodynamic calculated using the standard model is considered (Cropper et al. 1999), the observed strengths of the emission lines of various species and the model are in good agreement. The *XMM-Newton* RGS observations thus show strong support to the hydrodynamic scenario of the standard model.

Figure 5 shows the distribution of soft/hard X-ray ratios of AM Her systems obtained from the *ROSAT* survey by Ramsay et al. (1994) previously and from a recent *XMM-Newton* survey by Ramsay & Cropper (2004). The histogram corresponding to the *ROSAT* data indicates a large majority of the AM Her systems with a large soft/hard X-ray ratio (> 5). The *XMM-Newton* data, however, show a contradictive result: more than 50% of the systems have their soft/hard X-ray ratio smaller than 1. The discrepancy of the results from the two studies is obvious. Ramsay & Cropper (2004) argued that the high soft/hard X-ray ratio obtained in the
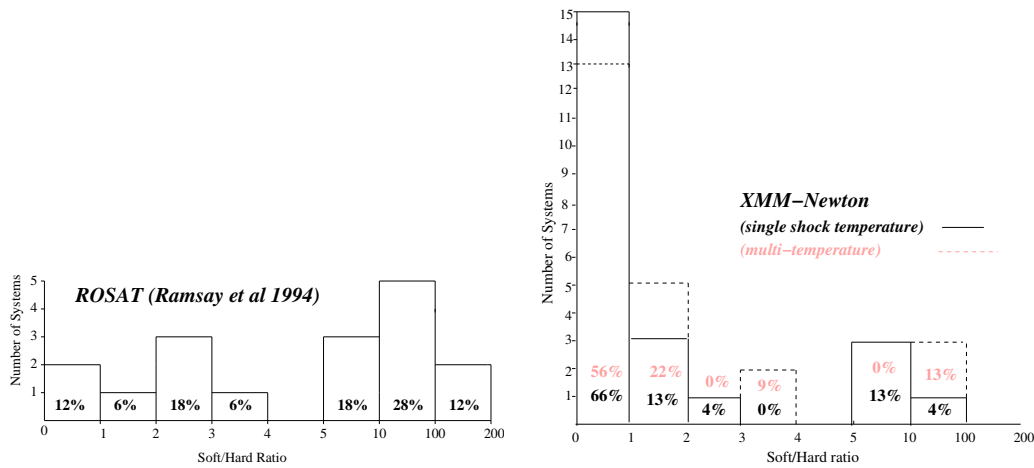
Fig. 5 The soft/hard X-ray ratio of AM Her systems (adopted from Ramsay & Cropper 2004). The histogram showing the ratio deduced from the *ROSAT* survey by Ramsay et al. (1994) is in the left, and the histogram showing the ratio deduced from the recent *XMM-Newton* survey is in the right.

presvious analysis of the *ROSAT* data were caused by a combination of factors, including the calibration of the data analysis software and the spectral models used in the fit. Their reanalysis of the *ROSAT* data revised that although only 1/5 of the AM Her systems showed excess of soft X-rays (with soft/hard X-ray ratio > 5), but the majority did not. The results of the *ROSAT* and the *XMM-Newton* observations thus reconcile. Moreover, AM Her systems generally have a soft/hard X-ray ratio allowed by the standard model.

4 ACCRETION STREAMS – GLOBAL STRUCTURES

While many studies of the post-shock accretion flow have been carried out, the accretion flow above the shock and the global properties of the whole accretion stream are not well investigated. It is generally accepted that the flow is channelled by the white-dwarf magnetic field to the magnetic pole regions, but the cross section and the footpoint locations of the accretion streams are somewhat uncertain. There is strong observational evidence that the footpoints of the accretion columns in AM Her are spatially extensive (Wickramasinghe et al. 1991) with cross sectional areas $\sim 10^{-5}$ of the surface area of the white dwarf. Determining the extent of the accretion stream and the footpoints have relied on modeling the optical polarization light curves. Early modelings were mostly trial-and-error and often involved other many subjective elements (see e.g. Ferrario & Wickramasinghe 1990). They also suffered from the degeneracy in the parameter space in the polarized cyclotron emission calculations (see e.g. Wu & Wickramasinghe 1990). More objective methods were developed only recently. Cropper & Horne (1994) considered the maximum entropy method and used the optical and X-ray light curves to map the emission region. The more promising Stokes imaging technique was proposed by Potter, Hakala & Cropper (1998) (based on a genetic algorithm), and it can produce maps for the footpoints of the accretion columns in an objective manner. The Stokes imaging technique is shown to be

robust, and it yields some interesting results, e.g. the accretion poles located on the opposite footpoints of the same set of dipole field lines in the AM Her system V347 Pav (Potter, Cropper & Hakala 2000).

To determine the three-dimensional spatial location of the accretion streams in mCVs is a great challenge to astronomers. It is important in several aspects. First of all, its location contains the information how the initial coupling between the accreting gas and the white-dwarf magnetic field occurs. Second, without knowing the trajectory of the stream, it is difficult to model the density and temperature structure in the accretion stream theoretically, as one needs this information to formulate the flow hydrodynamics and the irradiation heating. Most of the existing stream modeling studies assume a fixed stream trajectory, which consists of two arcs: one arc of varying opening angle connects the inner Lagrangian point of the binary to a coupling region at some distance from the white-dwarf surface, and from that region another arc following the dipole magnetic field lines to the white dwarf surface (see e.g. Harrop-Allin et al. 1999; Vrielman & Schwope 2001). A more recent development is the three-dimensional eclipse mapping using the genetically modified fireflies technique (Hakala, Cropper & Ramsay 2002). As this method dose not pre-assume the location of the coupling region, it allows us to study how the accretion flow begins to be confined by the white-dwarf magnetic field and determine the global properties of the accretion stream objectively.

5 SUMMARY

We review the standard model of magnetic-field confined accretion flow in mCVs with focus on the hydrodynamics and structures of the post-shock emission region. We assess the validity of the standard model in the view of recent X-ray observations. Some new techniques for the study of global properties of the accretion stream are briefly discussed.

References

Chanmugam, G., Barrett, P. E., Wu, K., Courtney, M., 1989, ApJS, 71, 323

Chevalier, R. A., Imamura, J. N., 1982, ApJ, 261, 543

Cropper, M., 1990, Sp. Sci. Rev., 54, 195

Cropper, M., Ramsay, G., Wu, K., 1998, MNRAS, 293, 222

Cropper, M., Wu, K., Ramsay, G., Kocabiyik, A., 1999, MNRAS, 306, 684

Cropper, M., Ramsay, G., Hellier, C., Mukai, K., Mauche, C., Pandel, D., 2002, Roy. Soc. of London Phil Tr. A, 360, 1951

Ferrario, L., Wickramasinghe, D. T., 1990, ApJ, 357, 583

Frank, J., King, A., Raine, D., 2002, Accretion Power in Astrophysics, 3rd Ed., Cambridge: Cambridge University Press

Fujimoto, R., Ishida, M., 1997, ApJ, 474, 774

Hakala, P., Cropper, M., Ramsay, G., 2002, MNRAS, 334, 990

Harrop-Allin, M. K., Hakala, P. J., Cropper, M. S., 1999, MNRAS, 302, 362

Heise, J. et al., 1985, A&A, 148, L14

Imamura, J. N., Wolff, M. T., Durisen, R. H., 1984, ApJ, 276, 607

Imamura, J. N., Durisen, R. H., Lamb, D. Q., Weast, C., 1987, ApJ, 378, 665

Imamura, J. N., Aboasha, A., Wolff, M. T., Wood, K. S., 1996, ApJ, 458, 327

Ishida, M., 1991, PhD Thesis, University of Toyko

Kuijper, J., Pringle, J. E., 1982, A&A, 114, L4

Lamb, D. Q., Masters, A. R., 1979, ApJ, 234, L117

Langer, S. H., Chanmugam, G., Shaviv, G., 1982, ApJ, 258, 289

Mewe, R., Kaastra, J. S., Liedahl, D. A., 1995, Legacy, 6, 16

Phillips, K. J. H., Mewe, R., Harra-Murnion, L. K., Kaastra, J. S., Beiersdorfer, P., Brown, G. V., Liedahl, D. A., 1999, A&AS, 138, 381

Potter, S. B., Hakala, P. J., Cropper, M., 1998, MNRAS, 297, 1261

Potter, S. B., Cropper, M., Hakala, P. J., 2000, MNRAS, 315, 423

Ramsay, G., Cropper, M., 2004, MNRAS, 347, 497

Ramsay, G., Mason, K. O., Cropper, M., Watson, M. G., Clayton, K. L., 1994, MNRAS, 270, 692

Saxton, C. J., 1999a, PhD Thesis, The University of Sydney

Saxton, C. J., 2002, PASA, 19, 282

Saxton, C. J., Wu, K., 1999b, MNRAS, 310, 677

Saxton, C. J., Wu, K., 2001, MNRAS, 324, 659

Saxton, C. J., Wu, K., Pongracic, H., Shaviv, G., 1998, MNRAS, 299, 862

Tennant, A. F., Wu, K., O'Dell, S. L., Weisskopf, M. C., 1998, PASA, 15, 339

Vrielmann, S., Schwope, A., 2001, MNRAS, 322, 269

Wada, T., Shimizu, A., Suzuki, M., Kato, M., Hoshi, M., 1980, Progr. Theor. Phys., 49, 776

Warner, B., 1995, Cataclysmic Variable Stars, Cambridge: Cambridge University Press

Wickramasinghe, D. T., Bailey, J., Meggitt, S. M. A., Ferrario, L., Hough, J., Tuohy, I. R., 1991, MNRAS, 251, 28

Woelk, U., Beuermann, K., 1996, A&A, 306, 232

Wu, K., 1994, PASA, 11, 61

Wu, K., 2000, Sp. Sci. Rev., 93, 611

Wu, K., Cropper, M., 2001a, MNRAS, 326, 686

Wu, K., Wickramasinghe, D. T., 1990, MNRAS, 246, 686

Wu, K., Cropper, M., Ramsay, G., 2001b, MNRAS, 327, 208

Wu, K., Chanmugam, G., Shaviv, G., 1994, ApJ, 426, 664